Earth Syst. Dynam. Discuss., 3, 643–682, 2012
www.earth-syst-dynam-discuss.net/3/643/2012/
doi:10.5194/esdd-3-643-2012

Earth System Dynamics Discussions

Detecting hotspots of atmosphere-vegetation interaction via slowing down – Part 1: A stochastic approach

S. Bathiany[1], **M. Claussen**[1,2], **and K. Fraedrich**[1,2]

[1]Max Planck Institute for Meteorology, KlimaCampus Hamburg, Germany
[2]Meteorologisches Institut, Universität Hamburg, KlimaCampus Hamburg, Germany

Received: 27 June 2012 – Accepted: 16 July 2012 – Published: 20 July 2012

Correspondence to: S. Bathiany (sebastian.bathiany@zmaw.de)

Published by Copernicus Publications on behalf of the European Geosciences Union.

Abstract

An analysis of so-called Early Warning Signals (EWS) is proposed to identify the spatial origin of a sudden transition that results from a loss in stability of a current state. EWS, such as rising variance and autocorrelation, can be indicators of an increased relaxation time (slowing down). One particular problem of EWS-based predictions is the requirement of sufficiently long time series. Spatial EWS have been suggested to alleviate this problem by combining different observations from the same time. However, the benefit of EWS has only been shown in idealized systems of predefined spatial extent. In a more general context like a complex climate system model, the critical subsystem that exhibits a loss in stability (hotspot) and the critical mode of the transition may be unknown.

In this study we document this problem with a simple stochastic model of atmosphere vegetation interaction where EWS at individual grid cells are not always detectable before a vegetation collapse as the local loss in stability can be small. However, we suggest that EWS can be applied as a diagnostic tool to find the hotspot of a sudden transition and to distinguish this hotspot from regions experiencing an induced tipping. For this purpose we present a scheme which identifies a hotspot as a certain combination of grid cells which maximize an EWS. The method can provide information on the causality of sudden transitions and may help to improve the knowledge on the susceptibility of climate models and other systems.

1 Introduction

The existence of potential tipping points in the climate system has received growing attention in recent years (Lenton et al., 2008; Lenton, 2011). In the narrower sense, a tipping point occurs when a system becomes very susceptible to an external forcing due to large positive feedbacks. In the extreme case the system's attractor disappears

ESDD
3, 643–682, 2012

at a threshold value of the forcing (bifurcation) and the state has to approach a different attractor.

In order to predict the collapse at a preconceived bifurcation or to distinguish such changes in stability from random state transitions, it has been proposed to exploit statistical precursors of instabilities (Wiesenfeld, 1985a,b, Wiesenfeld and McNamara, 1986), also called Early Warning Signals (EWS; Scheffer et al., 2009). The fundamental assumption behind their applicability is that the system is close to a deterministic solution and perturbed by small fluctuations which can be described as white noise. In case of the climate system this approach resembles Hasselmann's concept of stochastic climate models (Hasselmann, 1976). A common type of a bifurcation is the saddle-node bifurcation, where an eigenvalue approaches 0 (if time is continuous) as the system's stable fixed point loses stability. As a result, the linear relaxation time of the corresponding mode increases (Wissel, 1984). This phenomenon has recently been referred to as "critical slowing down" (Rietkerk et al., 1996; Scheffer et al., 2009; Ditlevsen and Johnsen, 2010; Dakos et al., 2010, 2011; Lenton, 2011; Lenton et al., 2012b). To avoid confusion with the phenomenon of algebraic (rather than exponential) decay in systems with second-order phase transitions (Strogatz, 1994) we will refer to the increased relaxation time simply as "slowing down". As a consequence of slowing down, the system's autocorrelation and variance can increase (Scheffer et al., 2009), and the spectrum is reddened (Kleinen et al., 2003). Considering nonlinear terms in the stability analysis, it follows that the skewness of the state variable can also increase in magnitude (Guttal and Jayaprakash, 2008).

However, the time scale of the external parameter change must be slow enough for the system to stay close to equilibrium and to allow sufficiently long time series for a statistically significant detection of EWS. A lack of detectability can thus impede any final conclusion on the existence of slowing down prior to an abrupt event. For example, Dakos et al. (2008) detected a consistent increase in autocorrelation with 95% probability in only 2 out of 8 paleo records (see their Table S3), and the results seem

ESDD
3, 643–682, 2012

to depend on the choice of the analysis method, parameter values and the particular proxy (Lenton et al., 2012a; Lenton et al., 2012b).

As the sampling error of EWS increases with autocorrelation, this problem becomes worse close to the tipping point (for example see Dakos et al., 2012). Better resolved time series may not always provide a solution as a sampling below the dynamic time scale of the system will not add relevant information.

To alleviate this problem, the use of spatial EWS has been suggested (Guttal and Jayaprakash, 2009; Donangelo et al., 2010; Dakos et al., 2010): in analogy to the time domain, spatial variance and cross-correlations between different units of a spatially explicit system, as well as the spatial correlation length increase towards a tipping point. As an estimate of spatial indicators only involves data from one particular time step, it is argued that the detection of slowing down can be more robust for spatial EWS. However, in these previous studies on spatial EWS, the system's boundaries are known and well-defined. In addition, the application of the one-dimensional concept of EWS to high-dimensional systems, though justified by theory (Ditlevsen and Johnsen, 2010; Sieber and Thompson, 2012), in practice requires a priori knowledge on the critical mode of the transition (Held and Kleinen, 2004). This critical mode indicates in which direction in phase space the bifurcation occurs and thus how the information should be combined to yield EWS.

In this study, we consider the case where both, the critical mode as well as the critical subsystem, are unknown. First, we demonstrate that under such general conditions EWS may not be detectable at any particular location of the system.

Second, we propose an alternative application of EWS: the diagnostic detection of critical regions of slowing down (hotspots) in time series.

The potential tipping point we analyse is the decline of North African vegetation cover in the mid-Holocene. In the Sahara and Sahel region, vegetation cover and precipitation are considered to be linked by a positive feedback on timescales beyond years (Claussen, 2009). The reasons are the effect of surface albedo on atmospheric stability (Charney, 1975), and the vegetation's contribution to water recycling (Claussen,

ESDD
3, 643–682, 2012

1997; Hales et al., 2004). In models with a large atmosphere-vegetation feedback, two stable equilibria can exist (Claussen, 1998; Brovkin et al., 1998; Zeng and Neelin, 2000; Wang and Eltahir, 2000; Irizarry-Ortiz et al., 2003) and the gradual change in orbital forcing can cause a sudden collapse in vegetation cover (Claussen et al., 1999; Liu et al., 2006).

Our study is structured as follows: in Sect. 2 we present a stochastic model of atmosphere-vegetation interaction which produces a vegetation collapse when a control parameter is varied. We then use the stochastic model to document a specific limitation of local EWS in a spatially explicit setting (Sect. 3). Based on this finding we explain our concept of a hotspot and present an algorithm for the detection of hotspots of slowing down (Sect. 4). We then discuss the performance of this algorithm for different properties of the analyzed time series and different parameter choices and conclude in Sect. 5 by discussing possible applications and limitations of our approach. An application of our method to the results of an atmosphere-vegetation model of intermediate complexity will be presented in a subsequent article.

2 A stochastic model of atmosphere-vegetation interaction

In order to test the performance of EWS-related methods, we generate time series with a simple stochastic model of vegetation dynamics in subtropical deserts. The structure of this model is similar to the conceptual model of Brovkin et al. (1998), Wang (2004), and Liu et al. (2006): annual precipitation P is a linear function of vegetation cover V, while equilibrium vegetation cover V^* as a function of P is of sigmoidal shape (Fig. 1):

$$V^* = \begin{cases} 0 & \text{if } P < P_1 \\ 1 & \text{if } P > P_2 \\ 1.03 - \dfrac{1.03}{1 + \alpha \left(\dfrac{P - P_1}{\exp(\gamma\, \delta)} \right)^2} & \text{otherwise,} \end{cases} \quad (1)$$

ESDD
3, 643–682, 2012

with

$$P_1 = \beta \exp(\gamma \delta/2)$$

$$P_2 = \beta \exp(\gamma \delta/2) + \frac{\exp(\gamma \delta)}{\sqrt{0.03\,\alpha}}.$$

This function is the result of a semiempirical fit to observations (Brovkin et al., 2002) and referred to as the original VECODE model in Bathiany et al. (2012b). Parameter values in all our simulations are $\alpha = 0.0011$, $\beta = 28$, $\gamma = 1.7 \times 10^{-4}$, and $\delta = 9100$. For all time series we analyse in this study, P is always between P_1 and P_2.

If the conditions of a specific region are described with only one value of each, V and P, the system's deterministic equilibria can be depicted as intersections of the green and blue curve in Fig. 1. Reducing the external parameter P_d describes the effect of decreasing Northern Hemisphere summer insolation during the mid-Holocene, leading to a decrease in precipitation. When the green equilibrium disappears the system experiences a saddle-node bifurcation and vegetation cover has to collapse to the remaining desert state.

We extend this conceptual model by defining V and P for several elements with index i (for example to represent different grid cells in a climate model). At each of the N elements equilibrium vegetation cover depends only on the local precipitation according to $V^*(P)$. Vegetation cover is updated every (yearly) timestep via the dynamic equation

$$V_i^{t+1} = V_i^t + \frac{V^*(P_i^t) - V_i^t}{\tau} + \sigma_V \eta_i^t. \quad (2)$$

Following Liu et al. (2006) we fix the time scale τ to 5 yr. Due to atmospheric water transport and circulation changes, local precipitation P_i at a particular time t depends

ESDD
3, 643–682, 2012

on vegetation cover at all elements:

$$P_i = \underbrace{P_{0_i} + s_i B}_{P_\mathrm{d}} + \sum_{j=1}^{N} \mathbf{k}_{ij} V_j + \sigma_P \eta_i \tag{3}$$

Due to the fast equilibration time of the atmosphere, Eq. (3) is not dynamic, and the V_i are all the state variables of this dynamical system. The system is globally coupled via $\mathbf{k}$ and in this regard differs from reaction-diffusion models with interactions between adjacent elements only. The choice of $V^*(P)$ and the interaction matrix $\mathbf{k}_{ij}$ determine the strength and spatial structure of the atmosphere-vegetation feedback and thus the stability properties of the system.

Brovkin et al. (1998), Wang (2004), and Liu et al. (2006) refer to the equilibrium precipitation in the absence of any vegetation as P_d. However, as P_d may differ at different elements, we split it into P_{0_i}, which is variable in space but not in time, and $s_i B$ with a scalar B as external control parameter. The local sensitivity of background precipitation to B is determined by parameters s_i, which are also variable in space, but not in time. In physical terms, B describes the effect of climate forcings, while the numbers we use are chosen arbitrarily.

The Gaussian white noise process η with small noise level σ is uncorrelated in space. We distinguish two types of noise but always use only one of them in our experiments: σ_V controls perturbations which are added to Eq. (2) directly (additive noise), while σ_P controls perturbations added to precipitation and whose impact on the state variable V_i depends on the system's state itself (multiplicative noise). Atmospheric variability is more realistically accounted for by the multiplicative noise case, whereas the additive noise case may describe disturbances other than atmospheric conditions, such as fire, diseases or grazing. Only the additive noise case allows rising variance to be a generic indicator of slowing down (Dakos et al., 2012), although we will show that in our specific model rising variance is also a useful indicator in the multiplicative

ESDD
3, 643–682, 2012

noise case. In all our simulations we use very small noise levels of $\sigma_V = 0.00013$ or $\sigma_P = 2\,\mathrm{mm\,yr^{-1}}$.

3 Performance of Early Warning Signals (EWS) in spatially coupled systems

In the following, we address the limitations of EWS at individual elements in a spatially inhomogenous setting. All statistical indicators are calculated from time series of the state variables V_i. Autocorrelations are determined for lag 1, crosscorrelations for lag 0.

3.1 First example: induced tipping

Consider the following simple system (system 1): 2 elements are coupled in a way that the first element can be bistable due to a large local feedback between P and V. Precipitation at the second element depends on vegetation cover at the first element, but not vice versa. We implement this property by chosing the interaction matrix

$$\mathbf{k} = \begin{pmatrix} 300 & 200 \\ 0 & 0 \end{pmatrix}$$

and parameters

$$P_0 = \begin{pmatrix} 0 \\ 100 \end{pmatrix}$$

$$s = \begin{pmatrix} 1 \\ 0.1 \end{pmatrix}.$$

As B is reduced, element 2 (blue) collapses in response to the collapse of element 1 (red; Fig. 2a). The collapse of element 2 is thus not related to a substantial loss of its own stability. It rather experiences the transition as an induced tipping caused by a

ESDD
3, 643–682, 2012

sudden change in external conditions that are imposed by element 1. The stability of element 2 is hardly affected by B directly as the difference in s_1 and s_2 indicates.

Therefore, element 1 shows a clear increase in autocorrelation (Fig. 2b) and variance (Fig. 2c) in the additive noise case, but element 2 does not. Only when the noise is multiplicative the system under consideration shows an increased variance (Fig. 2d; note that the scale differs from Fig. 2c by a factor 100), but results for autocorrelation are similar to the additive noise case. The increase in variance in the multiplicative noise case is specific to the conceptual model and results from the increasing sensitivity of V^* to precipitation changes when P is reduced (Fig. 1). Without any P-V-feedback ($\mathbf{k} = 0$) there would still be an increase in variance in the multiplicative noise case, but not in the additive noise case.

To obtain sufficiently precise estimates of the statistical properties in Fig. 2 we performed stationary time series of 10 million data points each for different values of B. In a transient situation where the sampling error is much larger, the collapse of element 2 would hardly be predictable with EWS.

3.2 Second example: collective bistability

To pursue this further, we now consider a system (system 2) with a different number of elements, distinguishing versions with 1, 2, 5, 10, and 20 elements, where any particular element has the identical parameters $P_{0_i} = 0$, $s_i = 1$, and $\mathbf{k}_{ij} = 300/N$. By dividing the entries of interaction matrix $\mathbf{k}$ by the number of elements in the system, we equally distribute the P-V-feedback over all elements. When more and more elements are coupled, the spatial resolution increases but the bifurcation diagram of this globally coupled system (Fig. 3a) does not change. As local feedbacks (determined by $\mathbf{k}_{ii}$) are weak, no single element is bistable anymore. This fact distinguishes our model from those in Guttal and Jayaprakash (2009), Dakos et al. (2010) and Donangelo et al. (2010), where individually bistable elements are coupled. However, the system as a whole still shows a bifurcation due to the spatial interactions $\mathbf{k}_{ij}$ with $i \neq j$.

ESDD
3, 643–682, 2012

As we couple more and more elements, it is evident that EWS like rising autocorrelation and variance at individual elements, as well as rising cross-correlation, tend to disappear (Fig. 3b–d). Again, variance in the multiplicative noise case (Fig. 3e) is an exception due to the increased slope in $V^*(P)$.

The one element-case here (red curves in Fig. 3) is identical to element 1 from the 2-element-mode (red curves in Fig. 2), and also to the system in Fig. 1 in Bathiany et al. (2012b). For EWS to appear properly like in this single element case, the system's time series need to be projected on the critical mode of the transition, a technique introduced as "degenerate fingerprinting" by Held and Kleinen (2004). The critical mode implies the direction in phase space in which the bifurcation occurs. Hence, if the critical mode of the transition is not known beforehand, the tipping can be unpredictable even in cases of very long time series.

4 Early Warning Signal – based hotspot detection method

So far we have chosen systems of simple structure. In a more general case like a spatially resolved climate model, the stability structure will be more complicated. Certain subsystems of the climate may show a loss of stability during a change in external forcing while the rest of the system may respond only indirectly, or even evolve independently. In Sect. 3 we documented that in multidimensional settings individual elements can fail to show EWS before a sudden transition. While this constitutes a caveat for the prediction of sudden transitions, one may make a virtue out of this caveat by using EWS to diagnostically infer information on the causality of a sudden transition. In terms of system 1, we aim at finding the nucleus of slowing down (hotspot) by distinguishing elements of the red and the blue kind. This is not possible by looking at the system's state directly, because red and blue elements collapse in synchrony. Of course, in complex systems there will be a continuum from red to blue and the definition of a threshold in between will be somewhat arbitrary. In principle, we expect that the hotspot can be identified as the combination of elements which (when projected on their critical mode)

ESDD
3, 643–682, 2012

maximizes an indicator of slowing down. In the following, we present an algorithm for hotspot detection which we apply to our stochastic model.

4.1 Highly idealized North African vegetation dynamics

As yet another example of the stochastic model framework in Sect. 2, consider 25 elements which can be interpreted as a highly idealized Northern Africa (Fig. 4). We refer to this system as system 3. Again we chose parameter values which lead to preconceived properties of the model: 5 of the 25 elements gradually become desert when B is reduced (brown elements). 5 elements stay mostly vegetated (green elements), a set of 9 elements becomes bistable and finally collapses due to a saddle-node bifurcation (red elements) and 6 elements substantially depend on the red ones but show a much weaker local atmosphere-vegetation feedback (blue elements; see Fig. 5). Elements with identical colours have identical parameter values and thus have the same state in equilibrium. Hence, there are 4 s_i and P_{0_i} (Table 1), and 16 $\mathbf{k}_{ij}$ (Table 2). In similarity to the examples in Sect. 3.2, no element is bistable on its own, as local feedbacks $\mathbf{k}_{ii}$ are too small. It is only due to the strong spatial interactions between the red elements that the system can bifurcate and thus show a vegetation collapse at $B \approx 43$.

The nucleus of the transition is the red area because this is where the system loses stability due to strong atmosphere-vegetation interaction. In the following, we refer to the red area as a hotspot.

4.2 Recipe for hotspot detection in case of additive noise

We now explain our method of analysis by applying it to system 3 with additive noise. The analysis is applied to several preferably long stationary time slices for fixed but different forcings B_j ($j = 1, 2, ..., J$) below the tipping point. Here we chose time series of vegetation cover for $B_1 = 150$, $B_2 = 90$, $B_3 = 55$, and $B_4 = 43$ (vertical dashed lines in Fig. 5) with 100 000 yr each. All steps that follow are an analysis of these time series and do not involve the model which generated them. We now describe the individual

ESDD
3, 643–682, 2012

steps of the analysis by starting with part B in Fig. 6, as this part of the analysis corresponds to the original degenerate fingerprinting by Held and Kleinen (2004), without time aggregation:

B1. For a given part of the system with N_p elements, we select a subset of n elements from these N_p elements. We refer to the number of elements in the complete system as N (here: 25), and the number of elements in a part of the system as N_p.

B2. For the n selected elements we calculate the leading EOF (eigenvector of the correlation matrix which represents the largest variance) for the last simulation (here: B_4). The analysis is based on the assumption that this pattern resembles the critical mode, if the selected area is the hotspot. To construct the EOFs we use the freely-available linear algebra package LAPACK.

B3. We project the n time series of every time slice on this EOF. In case of the last simulation J this projection is the principal component of the EOF.

B4. We calculate an EWS, here the autocorrelation at lag 1 (AC), of the corresponding projections. The result is a curve of J points of AC versus B, just like those in Figs. 2b and 3b, but less well resolved.

To automatically compare the results for different areas, we expand this degenerate fingerprinting method with the following steps:

B5 As it is not the absolute value of AC but its increase which indicates slowing down, we shift the curve vertically in order to be 0 at $j = 1$.

B6 We integrate the AC change over B (calculate the area of the $J - 1$ segments). We do so to take into account not only the difference between the first and last B, but the whole evolution of AC as is suggested by our results in Fig. 2. We refer to this quantity as the signal.

ESDD
3, 643–682, 2012

We repeat steps B1–6 for all possible combinations of elements. If the N_p elements mentioned in step 1 represent the whole system under consideration ($N_p = N$), one can then determine the area with the maximum signal, or the areas with a signal above a certain threshold. However, this requires the calculation of $2^N - 1$ such signals (minus 1 because selecting 0 elements is not an option). This becomes unfeasible already for N beyond 10. Therefore, not all possible combinations can be calculated and we use an iterative selection process to decide which elements can be dropped from the analysis:

A. We randomly devide the whole system into a number of non-overlapping parts. The number of parts is calculated from the fixed parameter n_{max} via the ceiling function $\lceil \frac{N}{n_{max}} \rceil$. The number of parts is thus as small as possible for a given n_{max}. The size of each part is then determined by distributing the N elements as equally as possible, so that each N_p fulfills $2 <= N_p <= n_{max}$.

B. For each part, steps 1–6 are applied. As an example, imagine that system 3 is analyzed with $n_{max} = 3$. Hence, the system is subdivided into 9 parts, of which 7 parts contain 3 elements, and 2 parts contain 2 elements. Table 3 gives an example of all areas and their associated signals for a part which consists of elements 13, 18, and 23.

C. From a signal list like Table 3 the contribution of different elements can be disentangled, with the aim to drop unimportant elements from the analysis completely. For any specific element, we add up the signals of all areas this element is part of (last row, second column in Table 3), and refer to it as the element's weight. In our example, elements 13 and 18 belong to the hotspot, so they contribute much more to the signal than element 23, whose weight is therefore smaller. Element 23 should thus be more likely to be removed from the analysis. In principle, our selection process resembles the logic of a football world cup: each team (element) does not compete directly against every other team, but only against those of the same group (part). Only teams performing well enough in their group remain in the tournament.

ESDD
3, 643–682, 2012

D. As a criterion for removing elements we set a threshold weight which is adjusted interactively to prevent that too many elements are removed too early. Here, we set the initial threshold t_{ini} to 5 % of the maximum weight. The absolute value of this threshold depends on the maximum weight in each part. As long as no element can be removed in any part, we increase the threshold by $t_{inc} = 5\,\%$. If the threshold would reach or exceeded the maximum weight, we set the threshold to 99.5 %. If at least one element can be removed we reset the threshold to its initial value t_{ini}. In both cases, we repeat from step A with all the remaining elements.

This way, the considered number of elements is gradually reduced. The procedure ends as soon as one of the following conditions is true: (1) the total number of remaining elements is not larger than n_{max}, in which case the analysis is repeated one last time with one part only. (2) The relative threshold reaches 99.5 %, but still no elements can be removed because the remaining elements are too similar to be discriminated.

The procedure serves as a sieve in order to filter out the important elements with a feasible number of calculations. As the results depend on the random distribution of elements to different parts, they will be very similar but not completely identical when the analysis is repeated. The hotspot of slowing down can be identified if the time series is long enough (or if enough realizations are available), because the remaining elements at the end of the analysis tend to contribute most to slowing down.

To obtain more quantitative results, all signals calculated during the procedure can be collected in a sorted list for further analysis. Elements belonging to the hotspot tend to be part of the areas with the strongest signals and are on top of the list (Fig. 7). However, elements that have been removed early during the analysis are not well sampled. The method therefore only provides information on the nature of the hotspot, but less on the stability properties of the rest of the system.

ESDD
3, 643–682, 2012

4.3 Recipe for hotspot detection in case of multiplicative noise

Although the algorithm can be applied to time series from model 3 with multiplicative noise in exactly the same way, its performance can be improved compared to the additive noise case by making the following changes:

B2. To calculate an EOF we now use the covariance matrix instead of the correlation matrix.

B3. We calculate the leading EOF not only for the last time slice B_J, but also for all previous time slices from $j = 2$ to J. For every EOF_j, we project all time slices (from B_1 to B_j) on EOF_j. We then obtain J-1 curves of autocorrelation changes (Fig. 8).

B6. To compare the different areas, we perform a double integration. In terms of Fig. 8: first, we calculate the area under a curve with a certain colour for $\mathrm{EOF}_{B=90}$ (Fig. 8a), $\mathrm{EOF}_{B=55}$ (Fig. 8b), and $\mathrm{EOF}_{B=43}$ (Fig. 8c). The resuling trajectory of integrated AC changes is then again integrated over B. This way, not only the shape of the projection on the last EOF is accounted for, but also the shape of previous projections.

C. We devide the signal list in the set of signals above the current threshold and the set of signals below this threshold. All elements which are part of any area above the threshold remain, the other elements are removed. Hence, the threshold is directly applied to the signals itself without the calculation of weights. This measure allows a better discrimination of the elements. In the additive noise case, it cannot be applied, because there the maximum signal usually belongs to the complete area.

We will refer to the last three points as elimination rule 2, while the strategy in the additive noise case is referred to as elimination rule 1.

ESDD
3, 643–682, 2012

What motivates us to make these modifications? While for the additive noise case the AC's trajectories at the hotspot (red area) and the complete area always look alike (not shown), they differ substantially in the multiplicative case: At the hotspot the signal starts to emerge early, even when projecting on a leading EOF far from the tipping point (red curves in Fig. 8). This is not the case for the other areas because the variability of the system differs substantially from the critical mode. As variances at the hotspot are very small, the EOF pronounces other elements than the hotspot and slowing down will thus not be observed in the projection. Close to the tipping point, the variance at the hotspot increases not only due to slowing down, but also due to the multiplicative noise which enhances variance as vegetation cover decreases. Therefore, the relative increase in variance is particularly large at the hotspot. Close to the tipping point, the system's variability becomes dominated by the critical mode and slowing down can be seen in the complete as well as the hotspot area. By making the above changes we use this property of the system to better distinguish the elements from each other. As a result, the hotspot can be detected much easier than in the additive noise case. Using time series of 10 000 yr each, the hotspot is clearly visible in the signal list for $n_{max} = 5$ (Fig. 9).

4.4 Performance analysis

It has become obvious in the previous sections that the algorithm involves a number of options and parameter values which have to be chosen in advance. Also, the performance of the method will depend on properties of the original time series. For a quantitative comparison of the algorithm's performance under different conditions, we perform 500 Monte Carlo experiments for each condition, using lag-1-autocorrelation (Table 4) and relative variance increase (Table 5) as EWS.

In each experiment a new realization of the time series is generated with system 3 and then analyzed with the hotspot detection algorithm. Figure 10 shows a frequency distribution of elements which remain at the end of each experiment for the additive noise case and a time series length of 2000 yr. After the 500 repetitions we evaluate

ESDD
3, 643–682, 2012

which fraction f_1 of the $500 \times n_{max}$ potentially identified elements belongs to the hotspot, and which fraction f_2 of the actually obtained elements belongs to the hotspot. f_1 and f_2 can differ because it is not always n_{max} elements that remain in the end.

As a measure of the method's performance η we define for both variants of f:

$$\eta_{1,2} = (f_{1,2} - \frac{H}{N})/(1 - \frac{H}{N}), \quad (4)$$

with N as the size of the system (25) and H as the size of the hotspot (9). If we assume that all 25 elements have an equal chance to be selected, the probability for any obtained element to be part of the hotspot is $H/N = 9/25$. A detection which does not differ from this random case has performance 0.

If exactly n_{max} elements are returned in every experiment, a detection which only returns hotspot elements has performance 1 for both variants of f (which is of course only possible because we chose an n_{max} smaller than the hotspot). The expectation value for the frequency of every element would be 100 in case of performance 0 (the solid black line in Fig. 10), and $500 \times 5/9$ in case of performance 1 (end of vertical scale in Fig. 10). Potential deviations from n_{max} elements in the output can lead to performances lower than 0 and larger than 1 if we apply f_1.

The decision for 500 repetitions can be justified by bootstrapping our Monte Carlo results (Efron, 1979): for any list of 500 sets of residual elements we draw n sets and measure their performances. We calculate the standard deviation of the obtained performances for many different n. It turns out that for 500 repetitions the standard deviation is approx. 0.015, and rather independent of the parameter and time series properties. Therefore we round all performances in Tables 4 and 5 to 2 decimal places. Above 500 repetitions, the uncertainty of the performance decreases very slowly while the computation time for the Monte Carlo experiments increases beyond feasibility.

From the performances in Tables 4 and 5 as well as the qualitative appearance of the resulting signal lists we draw the following conclusions with regard to different parameter choices and time series properties:

ESDD
3, 643–682, 2012

– The initial threshold t_{ini} and increment t_{inc} should be chosen small (a few percent of the maximum signal). If they are larger, the calculation is faster and not necessarily worse in performance, but the signal list will not be well sampled. A better sampling of each element's contribution to the signal allows a clearer discrimination between the elements in figures like Figs. 7 and 9. Particularly low η_1 for some larger t_{inc} result from the effect that too many elements are removed at once after increasing the threshold.

– The maximum number of elements per part n_{max} can be chosen small for first results. The smaller n_{max}, the faster the algorithm. When repeating the analysis with larger n_{max}, the signal list gives an indication of the size of the hotspot (or hotspots). As long as the maximum signal in the list clearly increases with n_{max}, the number of elements which form a common hotspot is larger than n_{max}. As Figs. 7 and 9 document, the full hotspot may already be identified for n_{max} smaller than the hotspot, if t_{ini} and t_{inc} are small to allow a robustly sampled signal list.

– Each EOF can be calculated as an eigenvector of the system's covariance matrix or alternatively its correlation matrix. If based on the covariance matrix, elements with large variance will be emphasized. Whether this improves the performance of a hotspot detection generally depends on the system under analysis.

– The choice of time slices should cover a range of B where the changes in steady state are already pronounced to achieve a good signal to noise ratio.

– The best definition of a signal and the best elimination rule depend on the system. In general, other strategies than ER 1 and 2 could be devised that may be taylored to a specific system. Although ER 1 should be applicable to any system, it may not lead to the most robust results as our multiplicative noise case demonstrates.

– Other EWS than autocorrelation can be used within the same framework. Relative increases in variance usually show better performances (Table 5) because of a larger signal-to-noise ratio (also see Ditlevsen and Johnsen, 2010).

ESDD
3, 643–682, 2012

– The length T of the time series as compared to the key variable's time scale τ has a major influence on the method's performance. As the time series provide only a limited sample, the performance will increase with T. If a single available realization of the time series is too short, the statistical properties of the variations are unsufficiently sampled and a hotspot detection can yield wrong results. It should therefore be checked whether the identified hotspot is robust to T by comparing different parts of the time series. Methods of block bootstrapping suited for time series (Politis, 2003) could in principle be applied to the full analysis to derive uncertainty estimates.

5 Summary and conclusions

By applying a simple stochastic model we have demonstrated that EWS at individual elements of a coupled system are no generic precursors of a sudden transition at a tipping point. If the local feedback of a particular element is weak or if the element's tipping is induced by other elements, EWS are not apparent until the bifurcation parameter is very close to its critical point. In this case the signal cannot be called early anymore, and a prediction of a sudden transition, together with the area where it will occur, must fail. On the other hand, we documented that indicators of slowing down can potentially be used to infer knowledge on the causality of a sudden transition from sufficiently long time series. To this end, we devised an algorithm to detect the hotspot or hotspots of slowing down in a many-element system. As slowing down indicates a loss in stability of the current state, the detected hotspot indicates a region where the system's susceptibility to perturbations becomes large.

Although our system is meant to represent the vegetation-atmosphere interaction in Northern Africa, the method of analysis is generic in the sense that it can be applied to any system satisfying the basic assumptions common to EWS approaches:

– The system is supposed to be close to a deterministic state (in terms of dynamical systems, a slow manifold), which loses stability.

ESDD
3, 643–682, 2012

– The system's variability results from small white noise.

It should be noted that the existence of a bifurcation is not a prerequisite of our method. Even in the case of weaker feedbacks and a more gradual transition will a change in stability be reflected in slowing down. However, the detectability of the signal tends to decrease as compared to a bifurcation where the system approaches a random walk. The main difference to previous applications of EWS is that our method does not only calculate the magnitude of slowing down but also identifies the subsystem where it occurs.

In principle, a prediction of sudden transitions could also be attempted with this approach. As new data points become available, new EOFs and projections may be constructed. As for any prediction based on EWS it must of course be known in advance which maximum signal is to be expected (Thompson and Sieber, 2011). For example, autocorrelation only comes close to 1 when there is a bifurcation, but peaks at lower values in less extreme cases.

In addition, the very large data requirements imply a vast separation between the time scale of changing external conditions and the intrinsic time scale of the system, a condition that is not often satisified. For our system 3, several 10 000–100 000 yr long time slices (with the vegetation's time scale being 5 yr) were required for a robust hotspot detection. However, the method's performance generally depends on properties of the analyzed system. The stronger the slowing down and the more pronounced the hotspot, the easier its detection.

Although we focus on autocorrelation and temporal variability, other indicators of slowing down such as spatial variability could be applied within the same iterative framework and may lead to better performances. As our additive and multiplicative noise case illustrate, the more the analysis method is taylored to a specific system, the more a priori knowledge on the data generating process is needed. For example, variance may increase or decrease when approaching a threshold, depending on the system under consideration (Brock and Carpenter, 2010; Dakos et al., 2012).

ESDD
3, 643–682, 2012

Additional caveats are imposed by unaccounted or changing properties of the external noise, which would affect EWS (Carpenter and Brock, 2006; Scheffer et al., 2009; Ditlevsen and Johnsen, 2010). In particular, we have only used white noise which is uncorrelated in space. However, it would physically be more reasonable to account for spatial correlations in the atmospheric variability. This could reduce the detectability of hotspots, because correlations between the state variables could not be attributed to spatial interactions alone, but would partly result from correlations in the noise.

Other problems may arise in cases of large noise. The local stability of the deterministic state may not be represented well anymore in EWS, and the noise can lead to an early tipping. More fundamentally, the system's mean behaviour in the large noise regime may not reflect its deterministic structure anymore due to noise-induced transitions (Horsthemke and Lefever, 1984). The link between a system's susceptibility and statistical properties of its variability breaks down under such conditions.

Within these limitations, our results suggest an alternative applicability of EWS which may contribute to a better understanding of numerical models. In this regard our study is a concretion of Lenton's recent conclusion: "even if further research shows that early warning is unachievable in practice, it could still provide valuable information on the vulnerability of various tipping elements to noise-induced changes." (Lenton, 2011). To this end, more systematic studies on the performance of indicators of slowing down for different classes of models will be particularly beneficial.

Acknowledgements. SB is grateful to Reiner Lauterbach for his very kind and exceptionally clear explanations of mathematical issues, to Jin-Song von Storch for her helpful comments, and to Hermann Held for the instructive discussions. KF, Max Planck Fellow, acknowledges the support by the Max Planck Society. This work is funded by Deutsche Forschungsgesellschaft, Cluster of Excellence "CliSAP" (DFG EXC 177).

The service charges for this open access publication have been covered by the Max Planck Society.

ESDD
3, 643–682, 2012

References

Bathiany, S., Claussen, M., and Fraedrich, K.: Detecting hotspots of atmosphere-vegetation interaction via slowing down – Part 2: Application to a global climate model, Earth Syst. Dynam. Discuss., 3, 683–713, doi:10.5194/esdd-3-683-2012, 2012a.

Bathiany, S., Claussen, M., and Fraedrich, K.: Implications of climate variability for the detection of multiple equilibria and for rapid transitions in the atmosphere-vegetation system, Clim. Dynam., 38, 1775–1790, doi:10.1007/s00382-011-1037-x, 2012b. 648, 652

Brock, W. A. and Carpenter, S. R.: Interacting regime shifts in ecosystems: implication for early warnings, Ecol. Monogr., 80, 353–367, 2010. 662

Brovkin, V., Claussen, M., Petoukhov, V., and Ganopolski, A.: On the stability of the atmosphere-vegetation system in the Sahara/Sahel region, J. Geophys. Res.-Atmos., 103, 31613–31624, 1998. 647, 649

Brovkin, V., Bendtsen, J., Claussen, M., Ganopolski, A., Kubatzki, C., Petoukhov, V., and Andreev, A.: Carbon cycle, vegetation, and climate dynamics in the Holocene: experiments with the CLIMBER-2 Model, Global Biogeochem. Cy., 16, 1139, doi:10.1029/2001GB001662, 2002. 648

Carpenter, S. R. and Brock, W. A.: Rising variance: a leading indicator of ecological transition, Ecol. Lett., 9, 308–315, doi:10.1111/j.1461-0248.2005.00877.x, 2006. 663

Charney, J. G.: Dynamics of deserts and drought in the Sahel, Q. J. Roy. Meteor. Soc., 101, 193–202, 1975. 646

Claussen, M.: Modeling bio-geophysical feedback in the African and Indian monsoon region, Clim. Dynam., 13, 247–257, 1997. 646

Claussen, M.: On multiple solutions of the atmosphere-vegetation system in present-day climate, Global Change Biol., 4, 549–559, 1998. 647

Claussen, M.: Late Quaternary vegetation-climate feedbacks, Clim. Past, 5, 203–216, doi:10.5194/cp-5-203-2009, 2009. 646

Claussen, M., Kubatzki, C., Brovkin, V., Ganopolski, A., Hoelzmann, P., and Pachur, H. J.: Simulation of an abrupt change in Saharan vegetation in the mid-Holocene, Geophys. Res. Lett., 26, 2037–2040, 1999. 647

Dakos, V., Scheffer, M., van Nes, E. H., Brovkin, V., Petoukhov, V., and Held, H.: Slowing down as an early warning signal for abrupt climate change, Proc. Natl. Acad. Sci. USA, 105, 14308–14312, doi:10.1073/pnas.0802430105, 2008. 645

ESDD
3, 643–682, 2012

Dakos, V., van Nes, E. H., Donangelo, R., Fort, H., and Scheffer, M.: Spatial correlation as leading indicator of catastrophic shifts, Theor. Ecol., 3, 163–174, 2010. 645, 646, 651
Dakos, V., Kefi, S., Rietkerk, M., van Nes, E. H., and Scheffer, M.: Slowing down in spatially patterned ecosystems at the brink of collapse, Am. Nat., 177, E153–E166, doi:10.1086/659945, 2011. 645
Dakos, V., van Nes, E. H., D'Odorico, P., and Scheffer, M.: Robustness of variance and autocorrelation as indicators of critical slowing down, Ecology, 93, 264–271, doi:10.1890/11-0889.1, 2012. 646, 649, 662
Ditlevsen, P. D. and Johnsen, S. J.: Tipping points: early warning and wishful thinking, Geophys. Res. Lett., 37, L19703, doi:10.1029/2010GL044486, 2010. 645, 646, 660, 663
Donangelo, R., Fort, H., Dakos, V., Scheffer, M., and Van Nes, E. H.: Early warnings for catastrophic shifts in ecosystems: comparison between spatial and temporal indicators, Int. J. Bifurcat. Chaos, 20, 315–321, doi:10.1142/S0218127410025764, 2010. 646, 651
Efron, B.: 1977 Rietz Lecture – Bootstrap Methods – Another Look At the Jackknife, Ann. Stat., 7, 1–26, doi:10.1214/aos/1176344552, 1979. 659
Guttal, V. and Jayaprakash, C.: Changing skewness: an early warning signal of regime shifts in ecosystems, Ecol. Lett., 11, 450–460, doi:10.1111/j.1461-0248.2008.01160.x, 2008. 645
Guttal, V. and Jayaprakash, C.: Spatial variance and spatial skewness: leading indicators of regime shifts in spatial ecological systems, Theor. Ecol., 2, 3–12, doi:10.1007/s12080-008-0033-1, 2009. 646, 651
Hales, K., Neelin, J. D., and Zeng, N.: Sensitivity of tropical land climate to leaf area index: role of surface conductance versus albedo, J. Climate, 17, 1459–1473, 2004. 647
Hasselmann, K.: Stochastic climate models. 1. Theory, Tellus, 28, 473–485, 1976. 645
Held, H. and Kleinen, T.: Detection of climate system bifurcations by degenerate fingerprinting, Geophys. Res. Lett., 31, L23207, doi:10.1029/2004GL020972, 2004. 646, 652, 654
Horsthemke, W. and Lefever, R.: Noise-Induced Transitions, Springer, 1984. 663
Irizarry-Ortiz, M. M., Wang, G. L., and Eltahir, E. A. B.: Role of the biosphere in the mid-Holocene climate of West Africa, J. Geophys. Res.-Atmos., 108, 4042, doi:10.1029/2001JD000989, 2003. 647
Kleinen, T., Held, H., and Petschel-Held, G.: The potential role of spectral properties in detecting thresholds in the Earth system: application to the thermohaline circulation, Ocean Dynam., 53, 53–63, doi:10.1007/s10236-002-0023-6, 2003. 645

ESDD
3, 643–682, 2012

Lenton, T. M.: Early warning of climate tipping points, Nature Clim. Change, 1, 201–209, doi:10.1038/NCLIMATE1143, 2011. 644, 645, 663
Lenton, T. M., Held, H., Kriegler, E., Hall, J. W., Lucht, W., Rahmstorf, S., and Schellnhuber, H. J.: Tipping elements in the Earth's climate system, Proc. Natl. Acad. Sci. USA, 105, 1786–1793, doi:10.1073/pnas.0705414105, 2008. 644
Lenton, T. M., Livina, V. N., Dakos, V., and Scheffer, M.: Climate bifurcation during the last deglaciation?, Clim. Past, 8, 1127–1139, doi:10.5194/cp-8-1127-2012, 2012a. 646
Lenton, T. M., Livina, V. N., Dakos, V., van Nes, E. H., and Scheffer, M.: Early warning of climate tipping points from critical slowing down: comparing methods to improve robustness, Phil. Trans. R. Soc. A, 370, 1185–1204, doi:10.1098/rsta.2011.0304, 2012b. 645, 646
Liu, Z. Y., Wang, Y., Gallimore, R., Notaro, M., and Prentice, I. C.: On the cause of abrupt vegetation collapse in North Africa during the Holocene: climate variability vs. vegetation feedback, Geophys. Res. Lett., 33, L22709, doi:10.1029/2006GL028062, 2006. 647, 648, 649
Politis, D. N.: The impact of bootstrap methods on time series analysis, Stat. Sci., 18, 219–230, doi:10.1214/ss/1063994977, 2003. 661
Rietkerk, M., Stroosnijder, L., Prins, H., and Ketner, P.: Sahelian rangeland development: a catastrophe?, J. Range Manage., 49, 512–519, 1996. 645
Scheffer, M., Bascompte, J., Brock, W. A., Brovkin, V., Carpenter, S. R., Dakos, V., Held, H., van Nes, E. H., Rietkerk, M., and Sugihara, G.: Early-warning signals for critical transitions, Nature, 461, 53–59, doi:10.1038/nature08227, 2009. 645, 663
Sieber, J. and Thompson, J. M. T.: Nonlinear softening as a predictive precursor to climate tipping, Phil. Trans. R. Soc. A, 370, 1205–1227, doi:10.1098/rsta.2011.0372, 2012. 646
Strogatz, S.: Nonlinear Dynamics and Chaos. With Applications to Physics, Biology, Chemistry, and Engineering, Perseus Books Group, 1994. 645
Thompson, J. M. T. and Sieber, J.: Predicting climate tipping as a noisy bifurcation: a review, Int. J. Bifurcat. Chaos, 21, 399–423, doi:10.1142/S0218127411028519, 2011. 662
Wang, G. L.: A conceptual modeling study on biosphere-atmosphere interactions and its implications for physically based climate modeling, J. Climate, 17, 2572–2583, 2004. 647, 649
Wang, G. L. and Eltahir, E. A. B.: Biosphere-atmosphere interactions over West Africa. II: Multiple climate equilibria, Q. J. Roy. Meteor. Soc., 126, 1261–1280, 2000. 647
Wiesenfeld, K.: Noisy precursors of nonlinear instabilities, J. Stat. Phys., 38, 1071–1097, doi:10.1007/BF01010430, 1985a. 645

ESDD
3, 643–682, 2012

Wiesenfeld, K.: Virtual Hopf phenomenon – a new precursor of period-doubling bifurcations, Phys. Rev. A, 32, 1744–1751, doi:10.1103/PhysRevA.32.1744, 1985b. 645
Wiesenfeld, K. and McNamara, B.: Small-signal amplification in bifurcating dynamical systems, Phys. Rev. A, 33, 629–642, doi:10.1103/PhysRevA.33.629, 1986. 645
Wissel, C.: A universal law of the characteristic return time near thresholds, Oecologia, 65, 101–107, doi:10.1007/BF00384470, 1984. 645
Zeng, N. and Neelin, J. D.: The role of vegetation-climate interaction and interannual variability in shaping the African savanna, J. Climate, 13, 2665–2670, 2000. 647

ESDD
3, 643–682, 2012

Table 1. Parameters P_{0_i} and s_i in example system 3 for 4 different types of elements. Colours correspond to those in Fig. 4.

	red	blue	green	brown
P_0	−50	40	210	40
s	1.7	0.8	0.2	0.9

ESDD
3, 643–682, 2012

Table 2. Interaction matrix **k** of system 3, distinguishing 4 different types of elements. Colours correspond to those in Fig. 4. A number in some row A and column B stands for the impact of any single element of type B on any single element of type A (for example: impact of red on blue: 15, impact of blue on red: 5).

	red	blue	green	brown
red	27	5	10	10
blue	15	4	3	3
green	8	2	15	2
brown	2	3	2	5

ESDD
3, 643–682, 2012

Table 3. Example signal list for elements 13, 18 and 23 from system 3 (additive noise case).

area	signal × 1000
23	1.97
18	10.61
18, 23	10.74
13	12.27
13, 23	12.26
13, 18	17.48
13, 18, 23	17.50
weights (13,18,23):	59.51, 56.33, 42.47

ESDD
3, 643–682, 2012

Table 4. Performances of the hotspot detection scheme for different parameter choices and time series properties with lag-1-autocorrelation increase as EWS. ER stands for elimination rule (for an explanation of this and other options see text). Performances are calculated from fractions f_1, italic results in parenthesis from f_2 (see Sect. 4.4).

parameters for hotspot detection					time series properties						
ER	EOF	n_{max}	t_{ini}	t_{inc}	time slices B_i	τ	noise	T = 1000	T = 2000	T = 5000	T = 10000
1	corr.	5	5 %	5 %	(150, 90, 55, 43)	5	add.	0.16 (*0.22*)	0.27 (*0.33*)	0.41 (*0.50*)	0.56 (*0.69*)
1	covar.	5	5 %	5 %	(150, 90, 55, 43)	5	add.	0.13 (*0.19*)	0.24 (*0.30*)	0.43 (*0.54*)	0.54 (*0.68*)
1	corr.	5	5 %	5 %	(150, 90, 55, 43)	2.5	add.	0.29 (*0.36*)	0.40 (*0.48*)	0.55 (*0.70*)	0.66 (*0.84*)
1	corr.	3	5 %	5 %	(150, 90, 55, 43)	5	add.	0.19 (*0.22*)	0.29 (*0.34*)	0.44 (*0.51*)	0.58 (*0.67*)
1	corr.	7	5 %	5 %	(150, 90, 55, 43)	5	add.	0.13 (*0.18*)	0.24 (*0.31*)	0.39 (*0.49*)	0.49 (*0.60*)
1	corr.	5	5 %	5 %	(300, 200, 100, 75, 43)	5	add.	0.10 (*0.13*)	0.13 (*0.18*)	0.23 (*0.30*)	0.37 (*0.46*)
1	corr.	5	5 %	5 %	(150, 90, 55)	5	add.	0.04 (*0.08*)	0.12 (*0.16*)	0.21 (*0.27*)	0.36 (*0.43*)
1	corr.	5	5 %	1 %	(150, 90, 55, 43)	5	add.	0.18 (*0.19*)	0.28 (*0.30*)	0.45 (*0.47*)	0.63 (*0.67*)
1	corr.	5	5 %	2,5 %	(150, 90, 55, 43)	5	add.	0.17 (*0.20*)	0.28 (*0.32*)	0.46 (*0.51*)	0.62 (*0.69*)
1	corr.	5	5 %	7,5 %	(150, 90, 55, 43)	5	add.	0.17 (*0.24*)	0.22 (*0.31*)	0.40 (*0.51*)	0.49 (*0.68*)
1	corr.	5	5 %	10 %	(150, 90, 55, 43)	5	add.	0.13 (*0.23*)	0.20 (*0.31*)	0.37 (*0.53*)	0.47 (*0.70*)
1	corr.	5	5 %	12,5 %	(150, 90, 55, 43)	5	add.	0.12 (*0.23*)	0.21 (*0.35*)	0.32 (*0.52*)	0.44 (*0.67*)
1	corr.	5	5 %	15 %	(150, 90, 55, 43)	5	add.	0.08 (*0.23*)	0.21 (*0.37*)	0.28 (*0.56*)	0.37 (*0.70*)
1	corr.	5	5 %	17,5 %	(150, 90, 55, 43)	5	add.	0.08 (*0.24*)	0.17 (*0.37*)	0.30 (*0.54*)	0.41 (*0.67*)
1	corr.	5	5 %	20 %	(150, 90, 55, 43)	5	add.	0.11 (*0.27*)	0.19 (*0.37*)	0.30 (*0.54*)	0.27 (*0.69*)
1	corr.	5	5 %	30 %	(150, 90, 55, 43)	5	add.	-0.01 (*0.27*)	0.11 (*0.42*)	0.26 (*0.54*)	0.36 (*0.68*)
1	corr.	5	5 %	40 %	(150, 90, 55, 43)	5	add.	0.11 (*0.28*)	0.21 (*0.39*)	0.28 (*0.54*)	0.30 (*0.68*)
1	corr.	5	5 %	50 %	(150, 90, 55, 43)	5	add.	-0.08 (*0.31*)	0.05 (*0.39*)	0.27 (*0.51*)	0.44 (*0.59*)
1	corr.	5	5 %	100 %	(150, 90, 55, 43)	5	add.	0.10 (*0.27*)	0.23 (*0.33*)	0.37 (*0.47*)	0.46 (*0.54*)
1	corr.	5	80 %	5 %	(150, 90, 55, 43)	5	add.	0.12 (*0.27*)	0.25 (*0.39*)	0.41 (*0.53*)	0.56 (*0.69*)
2	covar.	5	5 %	5 %	(150, 90, 55, 43)	5	mult.	0.60 (*0.62*)	0.66 (*0.66*)	0.87 (*0.84*)	1.10 (*0.94*)
1	covar.	5	5 %	5 %	(150, 90, 55, 43)	5	mult.	0.29 (*0.36*)	0.44 (*0.53*)	0.61 (*0.71*)	0.74 (*0.87*)
2	corr.	5	5 %	5 %	(150, 90, 55, 43)	5	mult.	0.43 (*0.46*)	0.50 (*0.53*)	0.70 (*0.64*)	0.95 (*0.70*)
1	corr.	5	5 %	5 %	(150, 90, 55, 43)	5	mult.	0.31 (*0.38*)	0.40 (*0.48*)	0.56 (*0.65*)	0.67 (*0.81*)
2	covar.	5	5 %	5 %	(300, 200, 100, 75, 43)	5	mult.	0.57 (*0.62*)	0.64 (*0.66*)	0.71 (*0.71*)	0.82 (*0.79*)
2	covar.	5	5 %	5 %	(150, 90, 55)	5	mult.	0.68 (*0.69*)	0.74 (*0.75*)	0.87 (*0.85*)	1.09 (*0.96*)
2	covar.	5	5 %	5 %	(150, 90, 55, 43)	2.5	mult.	0.64 (*0.67*)	0.79 (*0.79*)	1.12 (*0.94*)	1.63 (*0.99*)

ESDD
3, 643–682, 2012

Table 5. As Table 4, but for relative variance increase as EWS.

parameters for hotspot detection					time series properties						
ER	EOF	n_{max}	t_{ini}	t_{inc}	time slices B_i	τ	noise	T = 1000	T = 2000	T = 5000	T = 10 000
1	corr.	5	5 %	5 %	(150, 90, 55, 43)	5	add.	0.28 (*0.33*)	0.43 (*0.51*)	0.60 (*0.74*)	0.67 (*0.86*)
1	covar.	5	5 %	5 %	(150, 90, 55, 43)	5	add.	0.29 (*0.36*)	0.42 (*0.51*)	0.62 (*0.75*)	0.71 (*0.87*)
1	corr.	5	5%	5 %	(150, 90, 55, 43)	2.5	add.	0.38 (*0.45*)	0.53 (*0.63*)	0.67 (*0.83*)	0.73 (*0.94*)
1	corr.	5	5 %	1 %	(150, 90, 55, 43)	5	add.	0.31 (*0.33*)	0.48 (*0.50*)	0.69 (*0.72*)	0.81 (*0.85*)
1	corr.	5	5 %	2,5 %	(150, 90, 55, 43)	5	add.	0.32 (*0.35*)	0.45 (*0.50*)	0.64 (*0.71*)	0.76 (*0.86*)
1	corr.	5	5 %	7,5 %	(150, 90, 55, 43)	5	add.	0.27 (*0.36*)	0.41 (*0.51*)	0.57 (*0.73*)	0.62 (*0.87*)
1	corr.	5	5 %	10 %	(150, 90, 55, 43)	5	add.	0.28 (*0.39*)	0.41 (*0.56*)	0.51 (*0.74*)	0.59 (*0.86*)
1	corr.	5	5 %	12,5 %	(150, 90, 55, 43)	5	add.	0.22 (*0.36*)	0.35 (*0.55*)	0.48 (*0.74*)	0.60 (*0.88*)
1	corr.	5	5 %	15 %	(150, 90, 55, 43)	5	add.	0.20 (*0.38*)	0.31 (*0.55*)	0.42 (*0.75*)	0.54 (*0.87*)
1	corr.	5	5 %	17,5 %	(150, 90, 55, 43)	5	add.	0.19 (*0.38*)	0.28 (*0.57*)	0.45 (*0.74*)	0.56 (*0.86*)
1	corr.	5	5 %	20 %	(150, 90, 55, 43)	5	add.	0.25 (*0.43*)	0.33 (*0.56*)	0.34 (*0.75*)	0.23 (*0.88*)
1	corr.	5	5 %	30 %	(150, 90, 55, 43)	5	add.	0.10 (*0.42*)	0.21 (*0.51*)	0.42 (*0.74*)	0.50 (*0.85*)
1	corr.	5	5 %	40 %	(150, 90, 55, 43)	5	add.	0.20 (*0.39*)	0.30 (*0.54*)	0.33 (*0.74*)	0.27 (*0.88*)
1	corr.	5	5 %	50 %	(150, 90, 55, 43)	5	add.	0.06 (*0.43*)	0.24 (*0.51*)	0.45 (*0.65*)	0.54 (*0.71*)
1	corr.	5	5 %	100 %	(150, 90, 55, 43)	5	add.	0.22 (*0.35*)	0.36 (*0.45*)	0.49 (*0.59*)	0.57 (*0.70*)
1	corr.	5	80 %	5 %	(150, 90, 55, 43)	5	add.	0.27 (*0.43*)	0.41 (*0.55*)	0.60 (*0.74*)	0.69 (*0.87*)
2	covar.	5	5 %	5 %	(150, 90, 55, 43)	5	mult.	1.70 (*1.00*)	2.04 (*1.00*)	2.22 (*1.00*)	2.25 (*1.00*)
1	covar.	5	5 %	5 %	(150, 90, 55, 43)	5	mult.	0.68 (*1.00*)	0.53 (*1.00*)	0.32 (*1.00*)	0.37 (*1.00*)
2	corr.	5	5 %	5 %	(150, 90, 55, 43)	5	mult.	1.59 (*1.00*)	1.99 (*1.00*)	2.21 (*1.00*)	2.25 (*1.00*)
1	corr.	5	5 %	5 %	(150, 90, 55, 43)	5	mult.	0.69 (*1.00*)	0.50 (*1.00*)	0.31 (*1.00*)	0.36 (*1.00*)

ESDD
3, 643–682, 2012

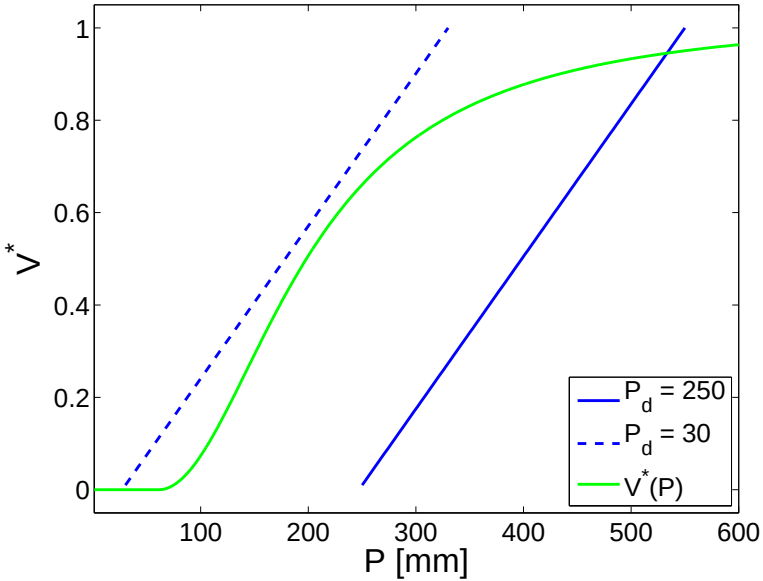

Fig. 1. Stability diagram for the one-dimensional conceptual model with $k = 300$ mm. Blue lines: equilibrium precipitation, calculated from $P^*(V) = P_d + kV$ for different P_d. Green line: equilibrium vegetation cover $V^*(P)$ (Eq. 1).

ESDD
3, 643–682, 2012

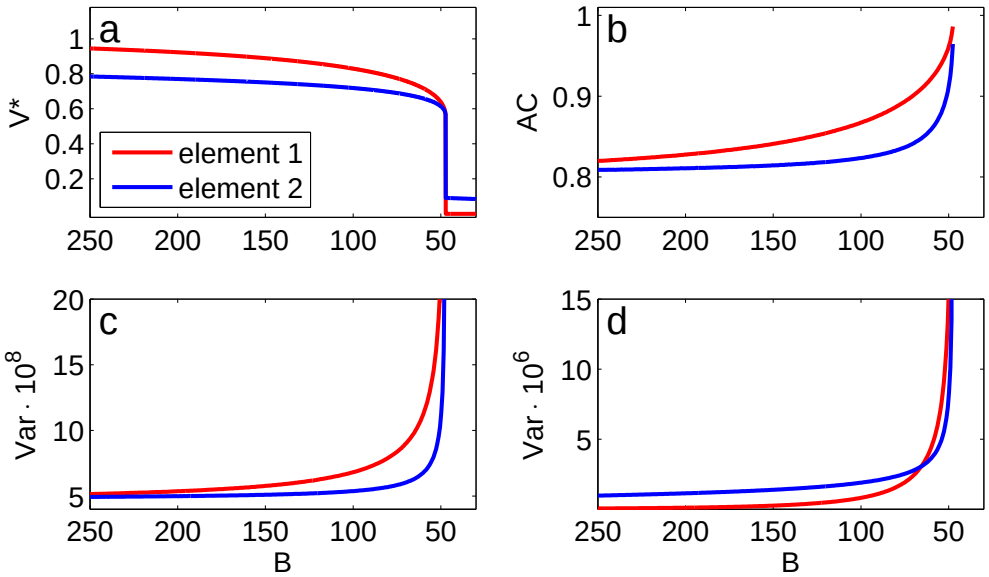

Fig. 2. Characteristics of system 1 in dependency on parameter *B*. **(a)** Equilibrium vegetation cover, **(b)** autocorrelation (lag 1), **(c)** variance (additive noise only), **(d)** variance (multiplicative noise only).

ESDD
3, 643–682, 2012

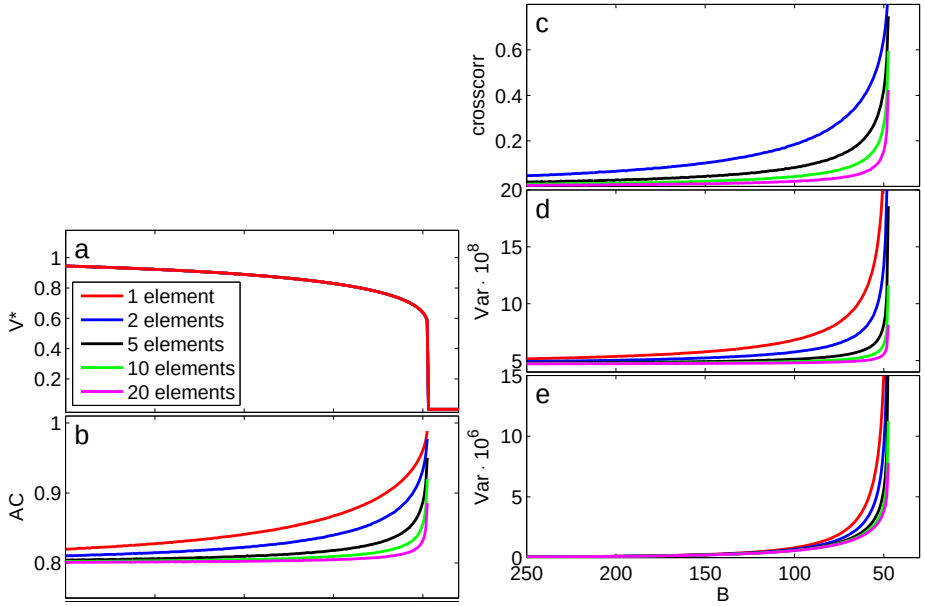

Fig. 3. Characteristics of system 2 in dependency on parameter *B* for versions with a different number of elements. **(a)** Equilibrium vegetation cover (identical for any number of elements), **(b)** autocorrelation (lag 1), **(c)** crosscorrelation (no lag), **(d)** variance (additive noise only), **(e)** variance (multiplicative noise only).

ESDD
3, 643–682, 2012

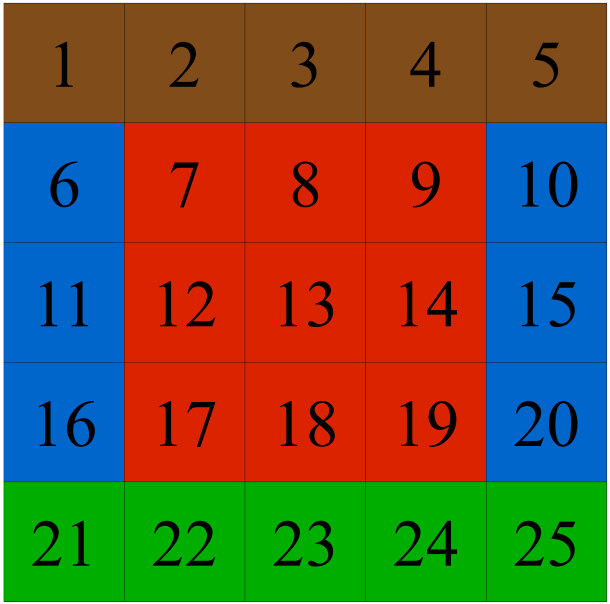

Fig. 4. Structure of system 3. Red: area with strong *P*-*V*-feedback (hotspot), blue: passively dependent on red area, brown: dry area, green: moist area.

ESDD
3, 643–682, 2012

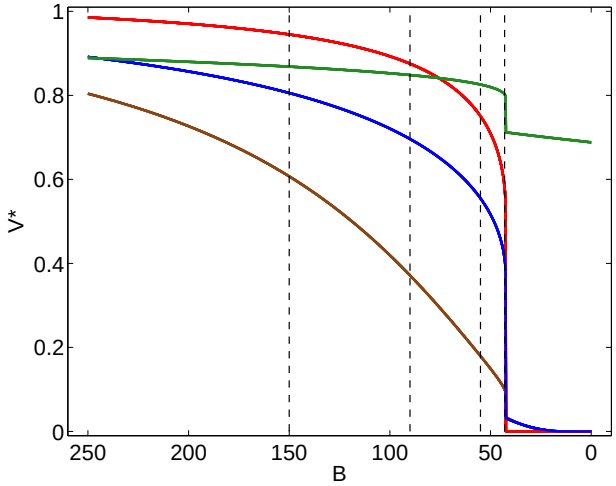

Fig. 5. Equilibrium vegetation cover at different elements of system 3 and for different bifurcation parameter values B. The colours correspond to the elements in Fig. 4. The vertical black dashed lines indicate the values of B used for the four stationary simulations (the smallest one also lying above the tipping point).

ESDD
3, 643–682, 2012

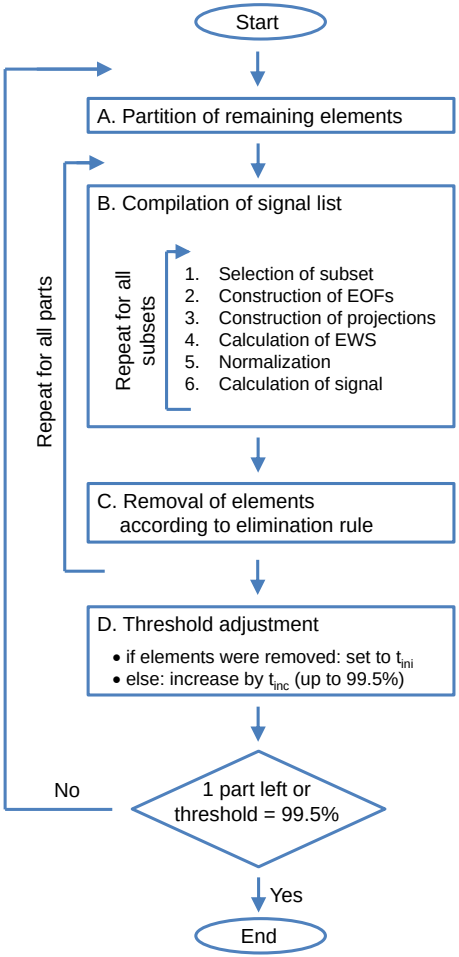

Fig. 6. General flowchart of the hotspot detection algorithm.

ESDD
3, 643–682, 2012

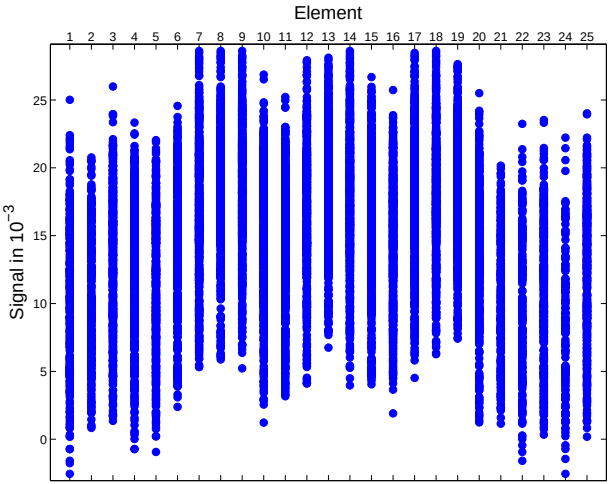

Fig. 7. Signal list for system 3 with additive noise using time series of 100 000 yr. Ordinate: absolute signal; abscissa: elements of the system. Any area that has been calculated during the analysis is represented at the ordinate value of its signal. All elements that are part of this area are marked as blue dots. Parameters are $t_{\mathrm{inc}} = 5\,\%$, $t_{\mathrm{ini}} = 5\,\%$, and $n_{\mathrm{max}} = 5$. The EOF is calculated from the correlation matrix.

ESDD
3, 643–682, 2012

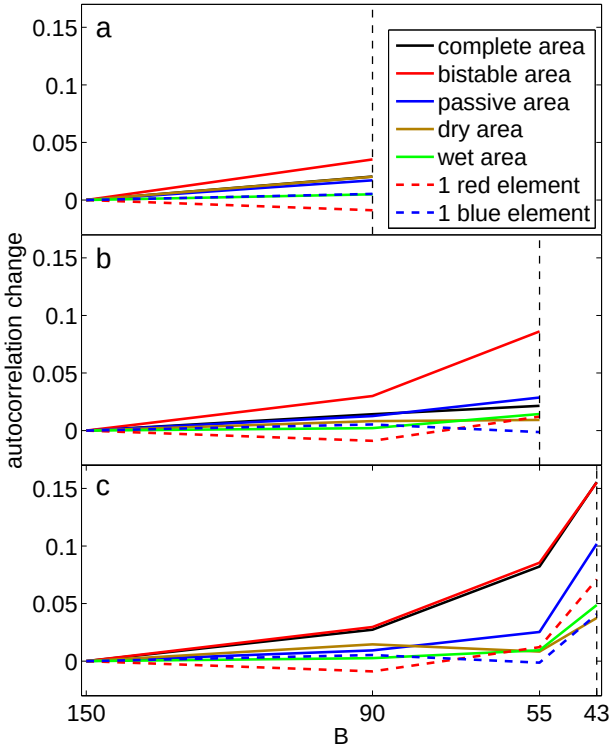

Fig. 8. Autocorrelation changes of projections on leading EOFs. The leading EOFs have been calculated for **(a)** $B_2 = 90$, **(b)** $B_3 = 55$, **(c)** $B_4 = 43$. In each case, all previous time series (including the one used for the EOF) are projected on the according EOF. The analysis is applied to the full system (black) as well as only parts of the system (other colours). The colours correspond to the elements in Fig. 4.

ESDD
3, 643–682, 2012

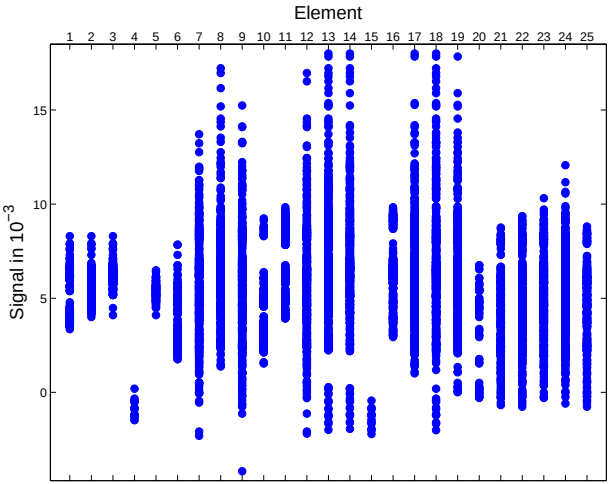

Fig. 9. Signal list for system 3 with multiplicative noise and time series of 10 000 yr. Ordinate: absolute signal; abscissa: elements of the system. Any area that has been calculated during the analysis is represented at the ordinate value of its signal. All elements that are part of this area are marked as blue dots. Parameters are $t_{\mathrm{inc}} = 5\,\%$, $t_{\mathrm{ini}} = 5\,\%$, and $n_{\mathrm{max}} = 5$. The EOF is calculated from the covariance matrix.

ESDD
3, 643–682, 2012

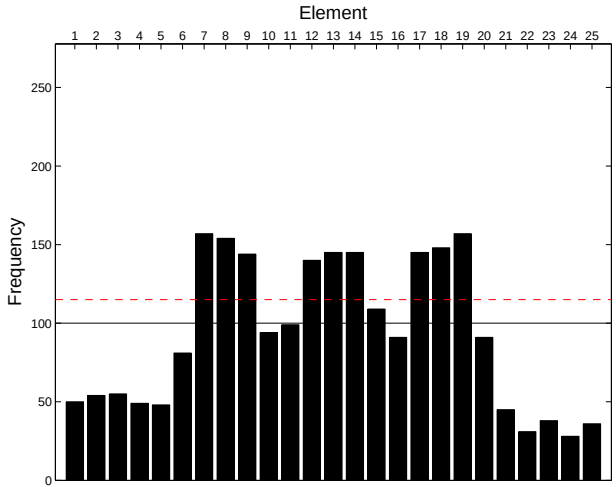

Fig. 10. Performance of the hotspot detection scheme for system 3 with additive noise using time series of 2000 yr. The frequencies show the number of times a particular element remains until the end of the selection process for 500 repetitions. Each repetition involves the generation of a new time series and its analysis with the hotspot detection algorithm. The solid black line marks the expectation value for a random selection where all elements are selected with equal probability. The red dashed line marks the 95% probability threshold of the corresponding cumulative binomial distribution. Parameters are $t_{\mathrm{inc}} = 5\,\%$, $t_{\mathrm{ini}} = 5\,\%$, and $n_{\mathrm{max}} = 5$. The EOF is calculated from the correlation matrix.

ESDD
3, 643–682, 2012